



ELSEVIER

Available online at www.sciencedirect.com

SCIENCE @ DIRECT®

Nuclear Instruments and Methods in Physics Research A 548 (2005) 336–354

NUCLEAR
INSTRUMENTS
& METHODS
IN PHYSICS
RESEARCH
Section A

www.elsevier.com/locate/nima

Comparison of high-energy electromagnetic shower profiles measured with scintillation and Cherenkov light

N. Akchurin^a, K. Carrell^a, J. Hauptman^b, H. Kim^a, A. Penzo^c,
R. Thomas^{a,1}, R. Wigmans^{a,*}

^aTexas Tech University, Lubbock, USA

^bIowa State University, Ames, USA

^cINFN Trieste, Italy

Received 11 June 2004; accepted 9 March 2005

Available online 1 June 2005

Abstract

Results are presented of detailed measurements of high-energy electromagnetic shower profiles measured in a copper-based fiber calorimeter. The calorimeter was equipped with a mixture of scintillating fibers and undoped (quartz or clear plastic) fibers. The latter measured Cherenkov light generated in the shower development process, whereas the scintillating fibers measured the energy deposit profile. Both lateral and longitudinal profiles were measured for electrons in the energy range 8–200 GeV. The scintillator and Cherenkov profiles exhibit some very striking differences, which are discussed and compared with results of Monte Carlo simulations.

© 2005 Elsevier B.V. All rights reserved.

PACS: 29.40.Ka; 29.40.Mc; 29.40.Vj

Keywords: Calorimetry; Electromagnetic shower profiles; Cherenkov light; Optical fibers

1. Introduction

The DREAM calorimeter was developed in the context of a generic R&D project, as a device that would make it possible to perform high-precision

measurements of hadrons and jets, while not subject to the limitations imposed by the requirements for compensating calorimetry [1]. The detector is based on a copper absorber structure, equipped with two types of active media which measure complementary characteristics of the shower development. Scintillating fibers measure the total energy deposited by the shower particles, while Cherenkov light is only produced by the charged, relativistic shower particles. Since the

*Corresponding author. Tel.: +1 806 742 3779;
fax: +1 806 742 1182.

E-mail address: wigmans@ttu.edu (R. Wigmans).

¹Now at KTech Corp., Albuquerque, USA.

latter are almost exclusively found in the electromagnetic (em) shower component (dominated by π^0 s produced in hadronic showers), a comparison of the two signals makes it possible to measure the energy fraction carried by this component, f_{em} , event by event. As a result, the effects of fluctuations in this component, which are responsible for all traditional problems in non-compensating calorimeters (non-linearity, poor energy resolution, non-Gaussian response function), can be eliminated. This leads to an important improvement in the hadronic calorimeter performance. The performance characteristics of this detector are described elsewhere [2–4].

The average shower shapes, longitudinal and lateral, have been measured by many groups, both for electromagnetic and hadronic showers, for a variety of absorber materials and particle energies. For example, Bathow and coworkers have measured longitudinal and radial profiles for 6 GeV electrons in lead, copper and aluminum in great detail [5]. Radial profiles at energies ranging from 10 to 150 GeV were measured by Acosta et al. for a lead/scintillating-fiber calorimeter [6], and Akchurin et al. measured longitudinal and lateral shower profiles for 0.5 GeV electrons in iron [7]. Our measurements offer the unique opportunity to compare the shower profiles measured with the relativistic shower particles (through the production of Cherenkov light) with those obtained from energy deposit measurements (scintillation), in otherwise identical experimental conditions. As it turns out, there are some striking differences between these profiles, which have consequences for the calorimetric measurements.

In Sections 2 and 3, we describe the calorimeter and the experimental setup in which it was tested. In Section 4, we discuss the experimental data that were taken and the methods used to analyze these data. Experimental results obtained from various data analyses are described and discussed in Section 5. These include longitudinal and lateral shower profiles measured with scintillation light and Cherenkov light. Differences between the results obtained with the two types of signals are emphasized. A summary and conclusions are presented in Section 6.

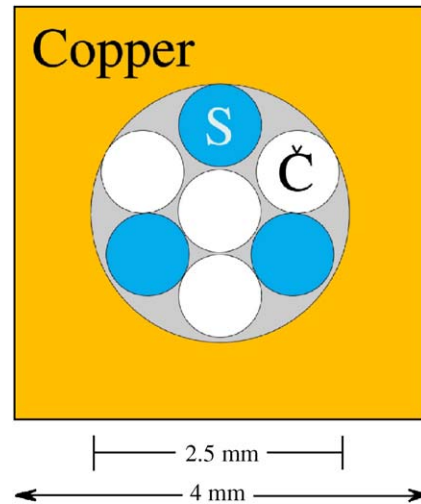


Fig. 1. The basic building block of the DREAM detector is a $4 \times 4 \text{ mm}^2$ extruded hollow copper rod of 2 m length, with a 2.5 mm diameter central hole. Seven optical fibers (four undoped and three scintillating fibers) with a diameter of 0.8 mm each are inserted in this hole, as shown.

2. The DREAM detector

The measurements described in this paper were performed with a calorimeter that has become known by its acronym DREAM, for Dual-READ-out Module. The basic element of this detector (see Fig. 1) is an extruded copper rod, 2 m long and $4 \times 4 \text{ mm}^2$ in cross-section. This rod is hollow, the central cylinder has a diameter of 2.5 mm. In this hole are inserted seven optical fibers. Three of these are plastic scintillating fibers,² the other four fibers are undoped fibers, intended for detecting Cherenkov light. We used two types of fibers for the latter purpose. For the central region of the detector, high-purity quartz fibers³ were used, while the peripheral regions of the detector were equipped with acrylic plastic fibers.⁴ The fiber pattern was the same for all rods, as shown in Fig. 1.

²SCSF-81J, produced by Kuraray Co. Ltd., Tokyo, Japan.

³Polymer-clad fused silica fibers, produced by Polymicro, Phoenix, AZ, USA.

⁴Raytela PJR-FB750, produced by Toray, Japan.

The DREAM detector consists of 5580 such rods, 5130 of these are equipped with fibers. The instrumented volume thus has a length of 2.0 m, an effective radius of $\sqrt{5130 \times 0.16/\pi} = 16.2$ cm and a mass of 1030 kg. The effective radiation length (X_0) of the calorimeter amounts to 20.10 mm, the Molière radius (ρ_M) is 20.35 mm and the nuclear interaction length (λ_{int}) 200 mm. The composition of the calorimeter is as follows: 69.3% of the detector volume consists of copper absorber, while the scintillating and Cherenkov fibers occupy 9.4% and 12.6%, respectively. Air accounts for the remaining 8.7%. Given the specific energy loss of minimum ionizing particles (mips) in copper (12.6 MeV/cm) and polystyrene (2.00 MeV/cm), the sampling fraction of the copper/scintillating-fiber structure for mips is thus 2.1%.

The fibers were grouped to form 19 towers. Each tower consists of 270 rods and has an approximately hexagonal shape (80 mm apex to apex). The effective radius of each tower is 37.1 mm ($1.82\rho_M$). A central tower is surrounded by two hexagonal rings, the Inner Ring (6 towers) and the Outer Ring (12 towers). The towers are longitudinally unsegmented. The readout structure is shown schematically in Fig. 2.

The depth of the copper structure is 200 cm, or $10.0 \lambda_{\text{int}}$. The fibers sticking out at the rear end of this structure were separated into 38 bunches: 19 bunches of scintillating fibers and 19 bunches of Cherenkov fibers. In this way, the readout structure was established. Each bunch was coupled through a 2 mm air gap to a photomultiplier tube (PMT).⁵ More information about this detector is given elsewhere [2,3].

3. Experimental setup

3.1. The beam line

The measurements described in this paper were performed in the H4 beam line of the Super Proton Synchrotron at CERN. The DREAM detector was mounted on a platform that could move vertically and sideways with respect to the beam.

⁵Hamamatsu R-580, 10-stage, 1.5" diameter.

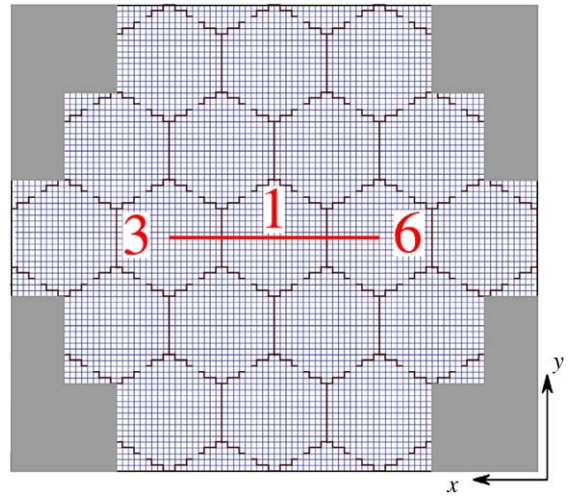


Fig. 2. Schematic layout of the DREAM calorimeter (front view). Each square represents a copper tube, shown in detail in Fig. 1. The subdivision into hexagonal readout towers is shown, while the area used for the position (x)-scan with 80 GeV electrons is indicated by the dark line running from the center of Tower 6 to the center of Tower 3.

Changing the angle of incidence of the beam particles with respect to the fibers in the horizontal plane (the ϕ angle) and the tilt angle (θ) was achieved with the intervention of a crane. For the measurements described in this paper, we used three different detector orientations:

- (A) Lateral profiles were obtained from measurements in which the angles ϕ and θ were 2° and 0.7° , respectively.
- (C) For the longitudinal profiles, the detector was rotated over an angle in the horizontal plane. Most data were taken at ($\phi = 24^\circ, \theta = 0$), where the detector entered the detector in Tower 17, as indicated in Fig. 3. This orientation was chosen since it allowed a measurement of the attenuation characteristics of the different types of fibers. It also made it possible to measure longitudinal shower profiles (including hadronic ones) over a depth of almost 1 m.
- (E) In a subsequent test period, the detector was rotated to the position ($\phi = 90^\circ, \theta = 0$), with the beam entering the detector in Tower 11, as indicated in Fig. 3.

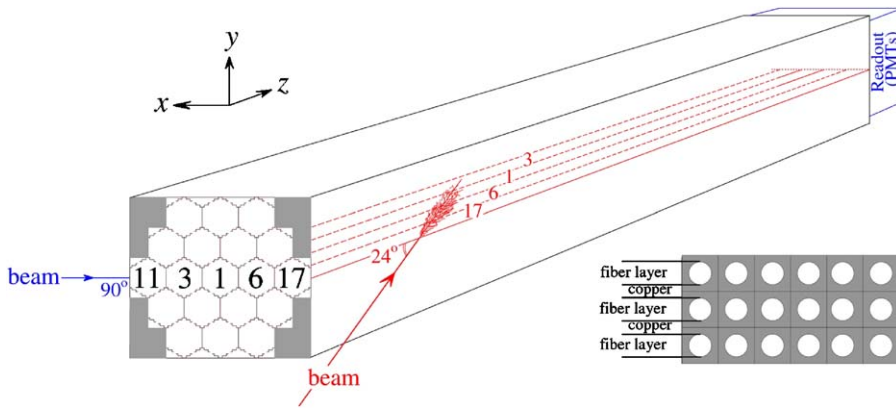


Fig. 3. Orientation of the DREAM calorimeter in positions $C(24^\circ, 0)$ and $E(90^\circ, 0)$. The electron beams entered the detector in the horizontal (x - z) plane, at an angle $\phi = 24^\circ$ or 90° with the direction of the fibers (the z -direction). The insert shows the fine-structure of the calorimeter, with horizontal fiber planes separated by layers of copper.

We used several auxiliary detectors in these beam tests. These detectors served to obtain clean samples of electron events and to measure the impact point of the particles in the calorimeter event by event.

Two small scintillation counters provided the signals that were used to trigger the data acquisition system. These Trigger Counters were 2.5 mm thick, and the area of overlap was $6 \times 6 \text{ cm}^2$. A coincidence between the logic signals from these counters provided the trigger.

The impact point of the beam particles in the DREAM detector was measured with a *fiber hodoscope*. This hodoscope consisted of ribbons of scintillating fibers oriented in the horizontal or vertical direction, thus providing the y and x coordinates of the beam particles. The fiber diameter was $500 \mu\text{m}$. Their signals were read out by means of multi-anode PMTs. This hodoscope was installed about 3 m upstream of the front face of the DREAM calorimeter. It was possible to determine the coordinates of the impact point in the calorimeter with a precision of a fraction of 1 mm, depending on the energy of the particles. More details about this hodoscope, and examples of its excellent performance, are given in Ref. [2].

The *preshower detector* consisted of a 5 mm thick ($1X_0$) lead absorber, followed by a scintillation counter. This simple device turned out to be

extremely useful to eliminate beam contamination and was an important tool in obtaining electron samples of high purity [2]. Downstream of the calorimeter, behind an additional $8\lambda_{\text{int}}$ of absorber, a $30 \times 30 \text{ cm}^2$ scintillator paddle served to identify muons that contaminated the particle beam.

3.2. Data acquisition

The various detector signals were transported through RG-58 cables with (for timing purposes) appropriate lengths to the counting room. There, the signals to be digitized (i.e. all except those from the trigger counters and the fiber hodoscope) were fed into charge ADCs. Two types of ADCs were used for these tests. Both types had a sensitivity of 4 counts/pC. The signals from the central tower and the Inner Ring were digitized by 11-bit Lecroy 2249W ADCs, which have a range of 500 pC. The signals from the 12 towers constituting the Outer Ring (see Fig. 2) were digitized by 10-bit Lecroy 2249 ADCs, which have a range of 250 pC. The duration of the gate opened by the trigger signal was 120 ns, and the calorimeter signals arrived ~ 30 ns after the start of the gate.

The signals from the fiber hodoscope were fed into TDCs. In total, eight TDCs were used, four for the horizontal and vertical fiber ribbons,

respectively. The time information could be converted into (x, y) coordinates of the point where the beam particle traversed the hodoscope.

The data acquisition system was based on CAMAC, interfaced via a VME bus to a Linux-based computer. At maximum, 8000 events could be recorded per SPS spill (total duration 14.4 s, beam extraction 2.6 s). The typical event size was ~ 150 bytes. All calorimeter signals, as well as the signals from all auxiliary detectors, could be monitored on-line.

3.3. Calibration of the detectors

Using the high voltage, the gain in the PMTs was set to generate ~ 2 pC/GeV in the central detector tower (Tower 1), ~ 4 pC/GeV in the Inner Ring (Towers 2–7) and ~ 6 pC/GeV in the Outer Ring (Towers 8–19) of the DREAM calorimeter. By choosing different gains, we effectively extended the limited dynamic range of our readout and thus increased its sensitivity to small energy deposits in the shower tails.

Each of the 19 towers was calibrated with 40 GeV electrons. The photomultiplier gains were chosen in such a way that the average signal for 40 GeV electrons entering in the center of a tower corresponded to about 300, 600 or 900 ADC counts above the pedestal value in that tower, depending on the chosen gain. On average, 92.5% of the scintillator light and 93.6% of the Cherenkov light was generated in that tower [2]. The signals observed in the exposed tower thus corresponded to an energy deposit of 37.0 GeV in the case of the scintillating fibers and of 37.4 GeV for the Cherenkov fibers. This, together with the precisely measured values of the average signals from the exposed tower, formed the basis for determining the calibration constants, i.e. the relationship between the measured number of ADC counts and the corresponding energy deposit. The stability of the calibration was checked four times during the test period by sending 40 GeV electrons into the center of each calorimeter tower and measuring the signal distribution. The mean values of these distributions were stable to within 2% in these measurements, for all channels.

4. Experimental data and methods

4.1. Experimental data

Events were triggered by coincident signals in the scintillation counters upstream of the calorimeter. Only events for which the (x, y) coordinates of the beam particle in the fiber hodoscope were measured were retained for the analyses described in this paper. One purpose of the hodoscope information was to be able to limit the impact region of the beam particles. For the analyses described in this paper, a circular region with a radius of 1.0 cm was selected.

The following data sets were used for these analyses:

- (1) Electron data at 8, 10, 20, 40, 80, 100, 150 and 200 GeV, taken with the detector oriented in position *C* ($24^\circ, 0^\circ$). These data were used to measure the (tails of) longitudinal electromagnetic shower profiles.
- (2) Electron data at 20 and 80 GeV, taken with the detector oriented in position *E* ($90^\circ, 0^\circ$). These data were used to measure the (first $15X_0$ of the) longitudinal electromagnetic shower profiles.
- (3) A scan with 80 GeV electrons was performed in 15 steps of 1 cm in the central region of the calorimeter, from the center of Tower 6 to the center of Tower 3 (see Fig. 2), with the calorimeter oriented in position *A* ($2^\circ, 0.7^\circ$). These data, and in particular those taken in positions near the boundaries between towers, were used for measuring the lateral electromagnetic shower profiles.

Pure electron samples were obtained using the information from the Preshower Detector and the Muon Counter. The procedures, as well as examples of the results achieved in this context, are described in Ref. [2].

4.2. Simulations

We have compared some of the results of our measurements with Monte Carlo simulations of electromagnetic shower development. We used the

EGS4 package for this purpose, as well as the GEANT3 program, which allows a detailed description of the detector geometry [8].

In the GEANT simulation, we defined discrete quartz and scintillation fibers. The generation of Cherenkov light was done exactly, as a function of charged particle velocity, for each photon in angle and wavelength. The numerical aperture was included and only those Cherenkov photons generated inside the quartz within the numerical aperture were kept. Scintillation light was generated isotropically along the length of the charged-particle track. The attenuation characteristics of the fibers and the quantum efficiency of the PMT as a function of wavelength were included in the simulations as well.

We also developed a separate, stand-alone simulation program that allowed us to study the relationship between the standard lateral shower profiles and the experimental data we obtained on lateral shower development (see Section 5.1).

5. Experimental results

5.1. Lateral shower profiles

Lateral shower profiles provide information about the energy deposit characteristics in a plane perpendicular to the shower axis. This information may be integrated over the full depth of the shower development, or it may concern a specific depth segment, e.g., the region around the shower maximum. Since the shower development is, on average, cylindrically symmetric, lateral shower profiles are best described in terms of dE/dr , the energy density as a function of the distance (r) to the shower axis. In that case, they are also called *radial profiles*.

Proper measurements of radial shower profiles require a detector with a cell size that is small compared to the characteristic features of that profile. The DREAM calorimeter does not qualify in that respect. One hexagonal cell contains on average more than 90% of the total shower energy deposited by an electron or photon that enters its central region.

However, the energy sharing between neighboring towers did provide important information about the energy deposit characteristics in a plane perpendicular to the shower axis. By varying the impact point of the particles, this energy sharing could be varied over a wide range. As we will see in the following, the profiles that can be extracted from this information are *not* the usual radial profiles dE/dr , but rather profiles that describe $\Delta E/\Delta x$, the energy deposited in a thin planar region located at a distance x from the shower axis (see Fig. 4). We will use the term *transverse profiles* for these.

A complicating factor in our measurements concerned the fact that the detector was oriented at a (small) angle with respect to the direction of the incoming particles. This led to a smearing effect which made it impossible to make accurate measurements at a very small distance from the shower axis. This can be seen as follows.

The impact point of the beam was varied in the x -direction (see Fig. 2). However, since the detector was oriented at an angle $\phi = 2^\circ$ with respect to the incoming particles, event-to-event fluctuations in depth (z) translated into a smearing in the x -coordinate. Since the fluctuations in depth occurred on the scale of one radiation length

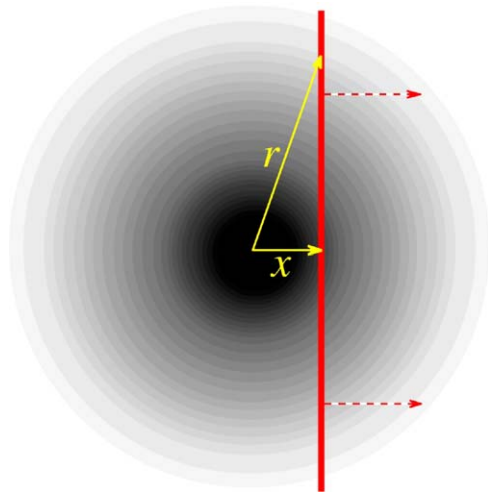


Fig. 4. Transverse shower profiles, $\Delta E/\Delta x$, measure the energy deposited in a thin planar region located at a distance x from the shower axis, as a function of x .

(20.1 mm), this smearing was of the order of $20.1 \sin 2^\circ = 0.7$ mm. Therefore, our profile measurements did not provide information on distance scales smaller than ~ 1 mm.

The transverse shower profiles were determined using data from the position scan, in which the 80 GeV electron beam was moved in steps of 1 cm across the central region of the calorimeter (data set 3, see Section 4.1). The measurements near the boundaries between Towers 1 and 3 provided the most detailed information. Fig. 5 shows this boundary region, together with circles representing the projection of the shower profile onto the x - y plane. The core of the shower, i.e. the black circle with radius r_1 , is fully contained in Tower 1 for this impact point, while the energy deposited between distances r_1 and r_2 is shared between Towers 1 and 3. Other towers, 2 and 4, also see signals from the peripheral shower tails ($r > r_2$).

As the impact point is moved to the right, Tower 1 sees an increasing fraction of the shower energy. This is illustrated in Fig. 6, where the calorimeter signals in Towers 1 and 3, averaged over 4 mm wide bins in the x -coordinate, are shown as a function of x . This averaging was necessary to eliminate the effects of systematic response differences between the signals from particles entering the calorimeter in the fiber planes or in the copper

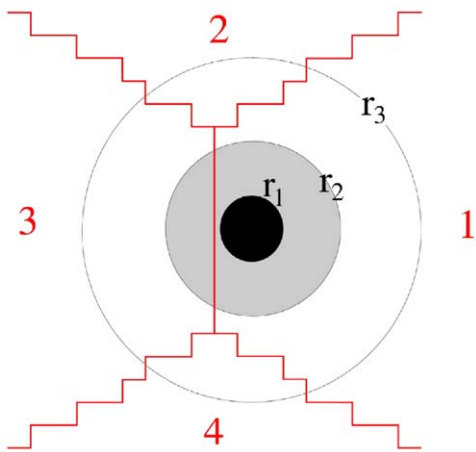


Fig. 5. An em shower developing near the boundaries between calorimeter towers. See text for details.

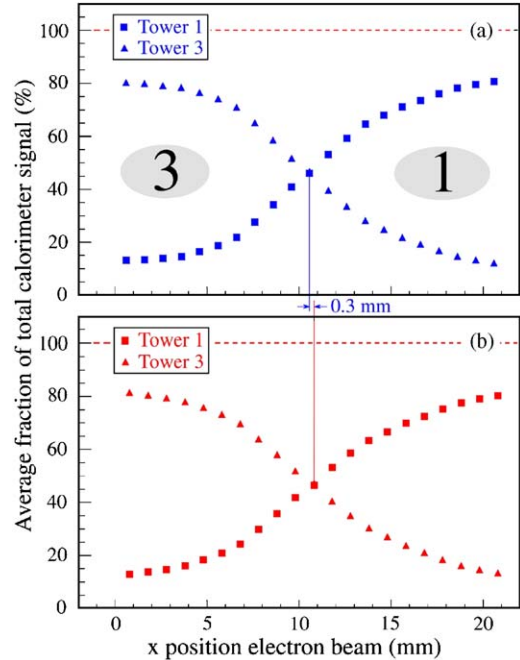


Fig. 6. Results of a position scan with 80 GeV electrons in the boundary region between Towers 1 and 3 (see Fig. 2). Shown are the average signals in these two towers, expressed as a fraction of the sum of the total calorimeter signal (i.e. the sum of all towers), as a function of the impact point of the particles. Each point represents the center of a bin with a width of 4 mm, the width of the copper tubes. Results are given for the signals from the scintillating (a) and the Cherenkov (b) fibers.

separating these planes. These differences are described and discussed in detail elsewhere [2].

If the shower development is cylindrically symmetric around the shower axis, then the difference between the average signals recorded in Towers 1 and 3 gives the fraction of the total signal that originated from a limited region surrounding that axis, at least in the approximation that the x - y plane is oriented perpendicular to the shower axis. This is conceptually illustrated in Fig. 7. Assuming that the circle represents the projection of the shower profile onto the x - y plane, the difference between the signals from Towers 1 and 3 is represented by the dark segment of this circle. This dark segment is a planar region (extending in the y - z directions) surrounding the shower axis. The width of this region is twice the distance (x_{13}) between the impact

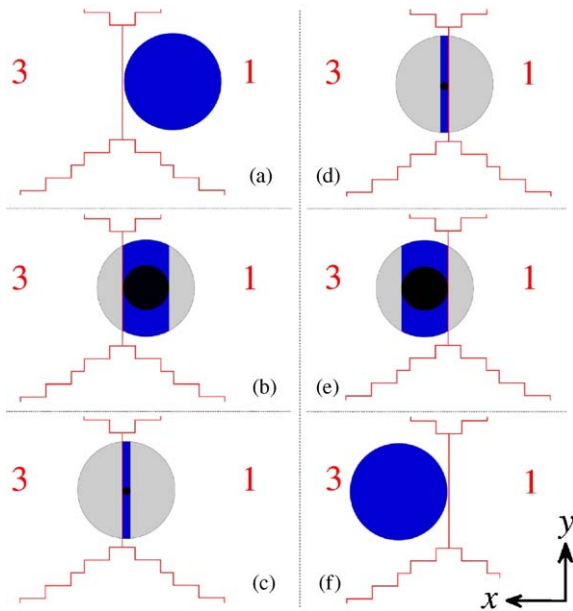


Fig. 7. Schematic depiction of results obtained from a position scan in the x -direction, in which the impact point of the particles moves across the boundary between Towers 1 and 3. The circle represents the projection of the shower profile onto the x - y plane. The dark region represents the fraction of the shower profile obtained by subtracting the signals from Towers 1 and 3 (see text for details).

point of the electrons and the boundary between Towers 1 and 3.

The experimentally observed difference between the average signals recorded in Towers 1 and 3 is shown in Fig. 8 as a function of the distance x_{13} . In order to correct for the effects of the fact that the angle ϕ was 2° in these measurements, we first determined the x -coordinate for which the signals in the two towers were exactly equal. Then, the results from measurements on both sides of the boundary were averaged. That is, the (absolute) signal differences between Towers 1 and 3 observed in Figs. 7b and e were averaged, and so were the signal differences observed in Figs. 7c and d.

In Fig. 8, experimental results are given separately for the scintillator and the Cherenkov signals. It is interesting to note that the values of the x -coordinate for which the average signals from Towers 3 and 1 were equal (the $x_{13} = 0$ reference point), were slightly different for the two

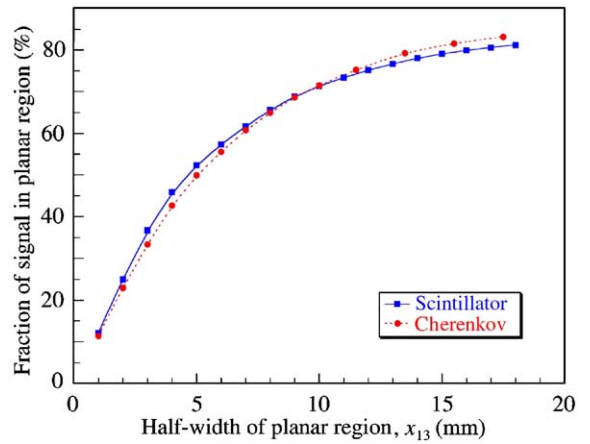


Fig. 8. The fraction of the total signal generated in a planar region surrounding the shower axis, as a function of the half-width of that region, i.e. the distance x_{13} between the shower axis and the region's boundaries. Results are given separately for the scintillator and the Cherenkov signals from 80 GeV electron showers.

types of signals. This is a reflection of the fact that the shower maximum was located somewhat deeper inside the absorber structure for the scintillator signals than for the Cherenkov ones (see Section 5.2). This translates, for an angle $\phi = 2^\circ$ and a 1 cm difference in shower maximum, into a 0.3 mm shift in the $x_{13} = 0$ reference point, in good agreement with the experimental data (Fig. 6).

Fig. 8 exhibits small, but very significant differences between the shower containment curves measured with the two types of signals. The data show that a planar region with a width larger than $2 \times 12 \text{ mm}^2$ generated a larger fraction of the total Cherenkov signal than of the scintillator signal. This is consistent with the observation that when electrons were steered into the center of a calorimeter tower, on average 93.6% of the total Cherenkov signal was recorded in that tower, vs. 92.5% of the total scintillator signal. The Cherenkov profile is thus narrower than the scintillator profile, at least for what concerns containment of the lateral shower tails. This can be understood from the fact that these tails are populated by particles produced in the late stages of the shower development. As the shower develops, the shower particles carry, on

average, less and less energy, and an increasing fraction of the shower particles falls below the Cherenkov threshold, where they can produce scintillation light, but no Cherenkov light.

However, Fig. 8 also shows that the situation is reversed very close to the shower axis. A planar region with a width of $2 \times 5 \text{ mm}^2$, surrounding the shower axis generated a significantly smaller fraction of the total Cherenkov signal than of the total scintillator signal. As discussed at the end of this subsection, this effect is a consequence of the very inefficient sampling of the early, narrow component of the shower development by the quartz fibers in this calorimeter. The virtual absence of a Cherenkov signal for this early, narrow shower component makes the fraction of the total scintillator signal coming from a region close to the shower axis larger than that for the Cherenkov signal. However, smearing effects resulting from the 2° angle, as well as contributions from areas at $r > x_{13}$ to the signals from our planar regions (see Fig. 4) tend to eliminate these differences. Yet, the data show that a planar region with a width of $2 \times 3 \text{ mm}^2$ generated 36.8% of the total scintillator signal, vs. 33.4% of the total Cherenkov signal.

Fig. 9 shows the *increments* ($\Delta E/\Delta x$) in the containment data as a function of the distance x_{13} . As discussed in the beginning of this section, these increments represent the energy contained in a 1 mm wide planar region extending in the y - z directions, located at a distance x_{13} from the shower axis (see also Fig. 4). Smearing effects resulting from the 2° angle limit the meaning of this profile for the area within a distance of $\sim 1 \text{ mm}$ from the shower axis, but the profiles at larger distances clearly show the difference between the scintillator and Cherenkov signals. These differences become especially clear when one looks at a logarithmic display of the data. Fig. 10a shows that the Cherenkov profile for $x > 1 \text{ mm}$ is well described by a single exponential, with a slope of about 6 mm. The scintillator profile (Fig. 10b) is also well described by an exponential with the same slope, but only for $x > 5 \text{ mm}$. Closer to the shower axis, this profile clearly exhibits a second component, which decreases steeper as a function of distance than the 6 mm component common to

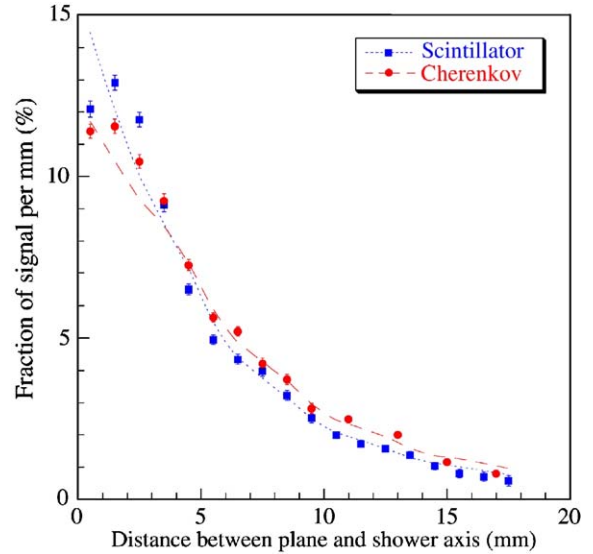


Fig. 9. Transverse shower profiles ($\Delta E/\Delta x$) for 80 GeV electrons. Shown is the fraction of the total signal generated in 1 mm wide planar regions, as a function of the distance (x) between these regions and the shower axis (see Fig. 4). Results are given separately for the scintillator and the Cherenkov signals from 80 GeV electron showers. The dashed and dotted lines represent the results of GEANT3 Monte Carlo simulations.

both profiles. A fit of a single exponential function to the experimental data ($x > 1 \text{ mm}$) resulted in a slope of 5.9 mm for the Cherenkov profile, with $\chi^2 = 49/11$. When an exponential function with this slope was fitted to the experimental scintillator data, the resulting χ^2 was found to be 275/16. On the other hand, an expression of the type

$$\frac{dE}{dx} = A_1 \exp(-x/\lambda_1) + A_2 \exp(-x/\lambda_2) \quad (1)$$

with λ_2 chosen as 5.9 mm, i.e. the same value as for the Cherenkov profile, gave the following fit results: $A_1 = 8.0$, $A_2 = 12.0$, $\lambda_1 = 2.5 \text{ mm}$, $\chi^2 = 75/14$.

The results of the fits are also shown in Fig. 10. The large χ^2 values of the fits are a consequence of the fact that only statistical errors on the mean values of the signal distributions were taken into account. These errors are very small, especially for the data points close to the shower axis. Systematic errors, for example resulting from uncertainties in the impact point of the particles

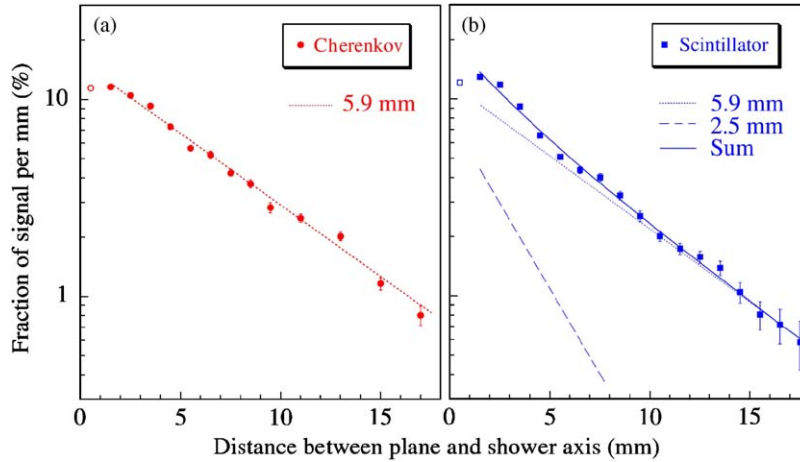


Fig. 10. Transverse shower profiles for 80 GeV electrons. Logarithmic display of the profiles measured with Cherenkov light (a) and scintillation light (b). The results of fits to the experimental data (only using points with $x > 1$ mm) are shown as well (see text for details).

and from fiber-to-fiber response variations are probably playing an important role as well. Nevertheless, the data show clearly that the Cherenkov profile is much better described by a single exponential than the scintillator profile.

At this point, it is necessary to examine the relationship between the radial shower profiles dE/dr and the (transverse) $\Delta E/\Delta x$ profiles measured in this study. For this purpose, we developed a simulation program that made it possible to determine the experimentally observed $\Delta E/\Delta x$ profile, starting from a chosen analytical expression for dE/dr . The energy deposit in 1 mm wide x -bins was calculated numerically, limiting the y -coordinate to values corresponding to the region covered by Towers 1 and 3 (see Fig. 5). It turned out that if dE/dr was chosen to decrease exponentially: $dE/dr = \exp(-\alpha r)$, $\Delta E/\Delta x$ was also well described by an exponential fit. The main difference was that the coefficient α was somewhat smaller in the latter case, to an extent determined by the steepness of the profile (i.e. the value of α) and the starting point (x_0) of the fit. For example, for the region $x_0 > 1.5$ mm, which was used for fits in our case, a slope in dE/dr of 2.5 mm became 2.8 mm in the $\Delta E/\Delta x$ profile, while a slope of 6.0 mm in dE/dr became 7.8 mm in $\Delta E/\Delta x$.

We conclude from these simulations that the characteristics observed for the $\Delta E/\Delta x$ profiles

(one exponential for the Cherenkov profile, a superposition of two exponentials for the scintillator profile) are essentially the same as for the dE/dr profiles, albeit that the parameter values in Eq. (1) are somewhat different for the two types of profiles. In particular, the ratio A_1/A_2 is smaller for the transverse profiles.

The observed lateral profile characteristics can be understood as follows. The lateral spread, and thus the radial profile of electromagnetic showers is determined by two distinctly different processes [1]:

- (i) Electrons and positrons move away from the shower axis because of multiple scattering.
- (ii) Photons and electrons produced in isotropic processes, in particular Compton scattering, move away from the shower axis. Compton scattering is important in this respect since the total photon absorption cross-section reaches a minimum in the energy range where this process dominates. As a result, the mean free path of Compton photons is considerably longer than the Molière radius (e.g., $1.7\rho_M$ for 1–3 MeV γ s in Cu).

These two processes give rise to a two-component radial energy deposit profile. This two-component profile structure was experimentally

established in great detail by Bathow and coworkers [5]. The steep multiple scattering component dominates the early part of the shower development, upstream of the shower maximum. Beyond the shower maximum, the radial energy deposit profile is dominated by the Compton scattering component.

Our measurements indicate that only the latter component plays a role for the Cherenkov signals. This can be understood from the fact that the steep multiple scattering component consists of energetic e^+e^- pairs produced by bremsstrahlung photons in the early stages of the shower development. These electrons/positrons travel in approximately the same direction as the beam electrons, i.e. almost parallel to the fibers. These particles do produce signals in the scintillating fibers. However, the Cherenkov light they emit falls outside the numerical aperture of the fibers and, therefore, this component is absent in the signals from the Cherenkov fibers.

5.2. Longitudinal shower development

The same phenomena that lead to differences between the lateral shower profiles measured with scintillation and Cherenkov light have also major consequences for the longitudinal characteristics. Longitudinal shower information was derived

from measurements in which the detector was rotated over an angle ϕ around its vertical axis. Two different angles were used for this purpose: 24° and 90° (see Fig. 3).

Fig. 11 shows the total scintillator and Cherenkov signal distributions for these two detector orientations, for 80 GeV electron showers. Three of the four distributions exhibit a clear doublet structure, which is caused by the fact that the sampling fraction, and thus the average calorimeter signal, depends on the impact point of the particles.

In Section 5.1, we saw that a considerable fraction of the shower energy is deposited very close to the shower axis, $\sim 15\%$ within a radius of 1 mm. Most of this energy is deposited in the early phase of the shower development, before the shower maximum is reached. The em shower starts as a very narrow beam, in which energy deposit is dominated by e^+e^- pairs produced by converting photons radiated by the primary electron. Given this characteristic, and the fact that the detector is not tilted ($\theta = 0^\circ$), the impact point of the beam particle is crucially important. Particles entering the detector in the copper layer separating two horizontal fiber layers (see inset Fig. 3) encounter essentially only copper during the first stage of their shower development. The early, collimated component of such showers is

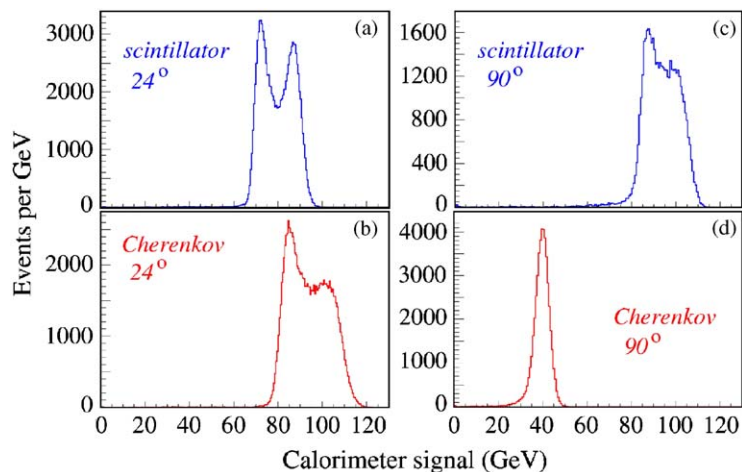


Fig. 11. Signal distributions for 80 GeV electrons measured with scintillation (a, c) and Cherenkov (b, d) light. The electrons entered the DREAM calorimeter at 24° (a, b) or at 90° (c, d).

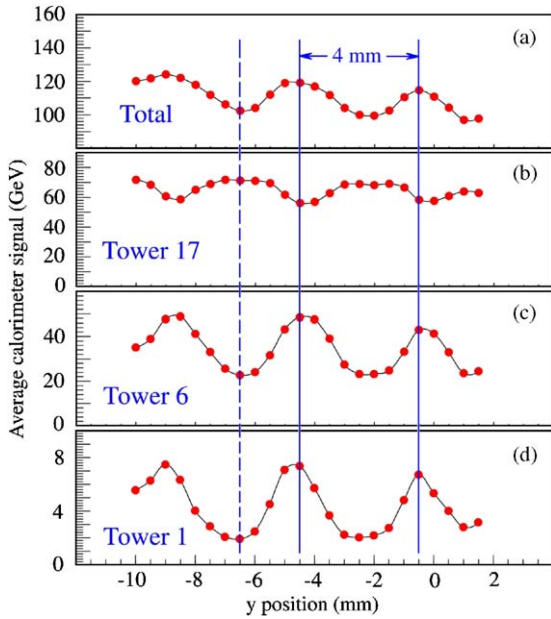


Fig. 12. Average scintillator signal as a function of the y -coordinate of the impact point, for 100 GeV electrons entering the DREAM calorimeter in position C ($24^\circ, 0$). Shown are the average total signal (a), as well as the average signals recorded in towers 17 (b), 6 (c) and 1 (d). The solid vertical lines correspond to positions where the electrons enter the calorimeter in a horizontal fiber plane. The dashed line indicates a position where the electrons enter the calorimeter in the copper layer in between such fiber planes. See Fig. 3 for geometric details.

thus much less efficiently sampled than for showers initiated by particles that enter the detector in the “Swiss cheese” part, i.e. in the horizontal fiber layers.

Evidence for this effect can be derived from Fig. 12a, which shows the total scintillator signal as a function of the y -coordinate of the impact point. The selected impact point area (a circle with a radius of 10 mm) was subdivided into y -bins of 0.5 mm width, using the hodoscope information. The total signal exhibits an oscillating pattern with a characteristic distance scale of 4 mm, i.e. exactly the transverse dimension of the tubes of which the DREAM calorimeter is composed (see Fig. 1). Detailed analysis of the distributions in the different towers contributing to the total signal (discussed in Section 5.3), proved that the minima and maxima of the total signal correspond to

impact points located in the copper and fiber planes, respectively.

The effects of this impact point dependence are observed for three of the four signal distributions shown in Fig. 11. However, it is completely absent in the Cherenkov measurements at 90° . At this angle, all Cherenkov light produced by the particles in the early, collimated shower component falls completely outside the numerical aperture of the fibers, regardless of the impact point of the particles. The only shower component detected in this geometry is the isotropic one, dominated by light emitted by Compton-scattered electrons. The latter component is much broader and, therefore, not noticeably dependent on the impact point of the beam particles.

At $\phi = 24^\circ$, a significant fraction of the Cherenkov light from the early, collimated component falls inside the numerical aperture of the fibers. Since the numerical aperture of the plastic fibers that detect this early shower component is 0.50, half of the opening angle of the cone around the shower axis that contains the trapped light amounts to 30° . Therefore, given the Cherenkov angle of 46° , light from this component will contribute to the calorimeter signals for ϕ angles ranging from 16° to 76° [9], when $\theta = 0$ (i.e., no tilt).

5.3. Longitudinal shower profiles

Longitudinal shower profiles were obtained from the energy sharing between the different calorimeter towers in the two geometries depicted in Fig. 3, in which the beam electrons entered the detector at 24° and 90° with the fiber direction, respectively.

Inspection of the 24° geometry shows that the showering electrons deposit their energy in that case primarily in the four calorimeter towers they encounter along the shower axis: The towers numbered 17, 6, 1 and 3. In the 90° geometry, the shower axis traverses Towers 11, 3, 1, 6 and 17, respectively.

At an angle of 24° , the path of the shower axis through each of the mentioned towers has a length of $72 \text{ mm} / \sin 24^\circ = 177 \text{ mm}$. This corresponds to $8.8X_0$. In first approximation, the signals from the

mentioned towers represent four longitudinal segments with a depth of $8.8X_0$ each. However, reality is somewhat more complicated.

As we noted earlier, beam particles entering the detector in the copper layer separating two horizontal fiber layers encounter essentially only copper during the early stage of their shower development. For all practical purposes, the first longitudinal segment, Tower 17, is thus thicker than the average value of $8.8X_0$ for such showers. If the tower was made of massive copper, then the depth of this segment would be $177/14.3 = 12.4X_0$. Similarly, the effective thickness of the first segment would be less than average for electrons entering the detector in the “Swiss cheese” part, i.e. in the horizontal fiber layers.

Particles entering the calorimeter in the horizontal fiber planes thus deposit a much smaller fraction of their total energy in Tower 17 than do particles entering in the copper. In the latter case, the shower maximum is located inside Tower 17 and the deeper segments (Towers 6 and 1) only sample the tails of the showers. Particles entering in the fiber planes deposit a much smaller fraction of their total energy in Tower 17, thus yielding a smaller signal in this tower than the electrons entering in the copper. On the other hand, the energy fraction and thus the resulting signals are much larger in the deeper segments, Towers 6 and 1. And because the early, highly collimated portion of the shower is more efficiently sampled for the particles entering in the fiber planes, the *total* scintillator response is also larger in this case.

Figs. 12b–d depict the contributions of Towers 17, 6 and 1 to the total scintillator signal observed as a function of the y -coordinate of the impact point, for the 24° geometry. A comparison of these distributions reveals that maxima in the total response indeed correspond to maxima in the signals recorded in Towers 6 and 1, and *minima* in the signals from Tower 17. Based on the above considerations, we concluded from this that the maxima and minima observed in the total signal distribution correspond to impact points in the fiber and copper layers, respectively.

By separating the events into subsamples according to the y -coordinate of their impact point, we doubled the number of measurement

points on the longitudinal shower profile. We estimated that the effective depth of Tower 17 would increase from its average value of $8.8X_0$ to $10.5X_0$ for particles entering the detector in the copper between two horizontal fiber planes, and that also the second segment (Tower 6) would be slightly deeper than average: $9.5X_0$. On the other hand, for particles entering in the horizontal fiber planes, the effective thickness of Tower 17 was reduced to $7.8X_0$ and that of Tower 6 to $8.4X_0$.

In the 90° geometry, the towers traversed by the developing shower are considerably thinner than at 24° : 72 vs. 177 mm. On average, this corresponds to $3.6X_0$. Also here, the information on the profiles could be increased by separating the events into subsamples, based on the impact points of the particles. The effective thickness of the first detector segment (Tower 11 in this case) was estimated to be $2.5X_0$ or $5.0X_0$ for electrons entering the detector in a fiber plane or in a copper layer separating these planes, respectively.

It turned out that in the 24° geometry an even further refinement was possible because of a structural detector element. Upstream material traversed by the particles before entering the calorimeter consisted of the PSD and a 5 mm thick steel plate holding the copper tubes in place, in total $1.5X_0$ of material. However, the electron beams glanced a steel bar that was part of the detector frame. Part of the beam particles traversed this bar, which had a thickness of about one radiation length. Using the hodoscope information on the x -coordinate of the impact point, we could separate the events into subsamples that did or did not encounter this obstacle located right in front of the active detector mass and therefore traversed either $1.5X_0$ or $2.5X_0$ before entering the calorimeter proper. This procedure thus increased the number of measurement points on the longitudinal shower profile by another factor of two.

All the above information is summarized in Table 1, which lists the sections of the longitudinal shower profile sampled by the various towers for the different event samples described above, as well as the average depth of each section.

All available data were used to reconstruct the longitudinal profile shown in Fig. 13. This profile

Table 1

The effective depth range and average depth, in radiation lengths, of the various longitudinal segments of the DREAM calorimeter, for event samples with different impact points

Impact point, 24°	Tower 17	Tower 6	Tower 1	Tower 3	
Fiber plane, no frame	1.5–9.3 (5.4X ₀)	9.3–17.7 (13.5X ₀)	17.7–26.5 (22.1X ₀)	26.5–35.3 (30.9X ₀)	
Fiber plane, frame	2.5–10.3 (6.4X ₀)	10.3–18.7 (14.5X ₀)	18.7–27.5 (23.1X ₀)	27.5–36.3 (31.9X ₀)	
Cu plane, no frame	1.5–12.0 (6.8X ₀)	12.0–21.5 (16.8X ₀)	21.5–30.3 (25.9X ₀)	30.3–39.1 (34.7X ₀)	
Cu plane, frame	2.5–13.0 (7.8X ₀)	13.0–22.5 (17.8X ₀)	22.5–31.3 (26.9X ₀)	31.3–40.1 (35.7X ₀)	
Impact point, 90°	Tower 11	Tower 3	Tower 1	Tower 6	Tower 17
Fiber plane	1.0–3.5 (2.3X ₀)	3.5–6.5 (5.0X ₀)	6.5–10.1 (8.3X ₀)	10.1–13.7 (11.9X ₀)	13.7–17.3 (15.5X ₀)
Cu plane	1.0–6.0 (3.5X ₀)	6.0–10.0 (8.0X ₀)	10.0–13.6 (11.8X ₀)	13.6–17.2 (15.4X ₀)	17.2–20.8 (19.0X ₀)

The top table concerns the measurements performed at $\phi = 24^\circ$, the bottom table is for $\phi = 90^\circ$ (see text for details).

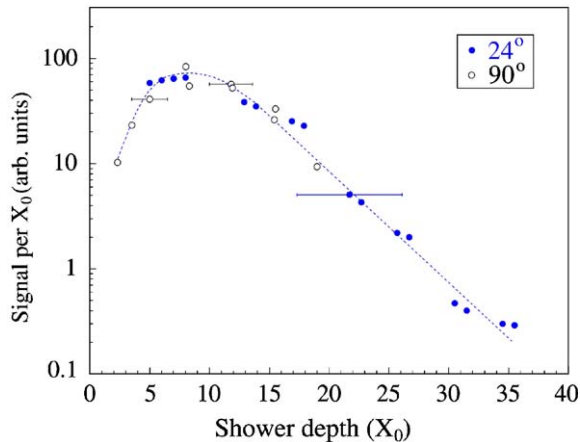


Fig. 13. The longitudinal shower profile for 80 GeV electrons, measured with the Cherenkov signals. The horizontal bars indicate typical bin sizes.

concerns showering 80 GeV electrons, registered through their Cherenkov signals. The 90° data probe the early part of the shower, up to a depth of $\sim 19X_0$, the 24° data mainly probe the part beyond the shower maximum. Each point represents the center of a horizontal bin. The widths of some representative bins are indicated in the figure.

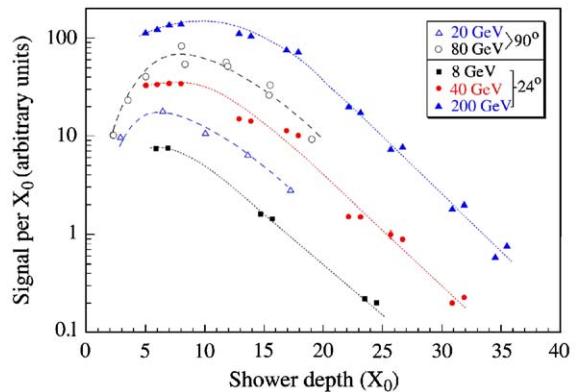


Fig. 14. Comparison of the longitudinal shower profiles for electrons of energies ranging from 8 to 200 GeV, measured with the Cherenkov signals. Some of the profiles were measured with electrons incident at 24°, others at 90°. The curves are drawn to guide the eye.

Fig. 13 shows indeed the typical, well known characteristics of electromagnetic shower profiles: A steep rise to the shower maximum, located at a depth of $\sim 8X_0$ in this case, followed by a less steep, more or less exponential decay. In Fig. 14, profiles measured for various electron energies, ranging from 8 to 200 GeV, are displayed. At low

energies (<40 GeV), the position resolution of the hodoscope was insufficient to distinguish effectively between particles entering the detector in the fiber or copper planes and, therefore, fewer data points were available. The figure shows that the exponential decrease beyond the shower maximum is essentially independent of the shower energy and that the main difference between these profiles concerns the fact that the shower maximum shifts to greater depth when the electron energy is increased.

These data illustrate that our measurements provided rather detailed information on the longitudinal em shower profiles. However, the primary goal of our study was to investigate possible differences between the profiles measured with the two signal sources of our calorimeter, scintillation light and Cherenkov light. Results on this are given in Figs. 15 and 16.

Fig. 15 shows results obtained for electrons entering the detector at 90° with the fiber direction. These measurements probe the early part of the shower development. The figure shows the ratio of the average Cherenkov and scintillator signals observed in the five towers (11, 3, 1, 6 and 17)

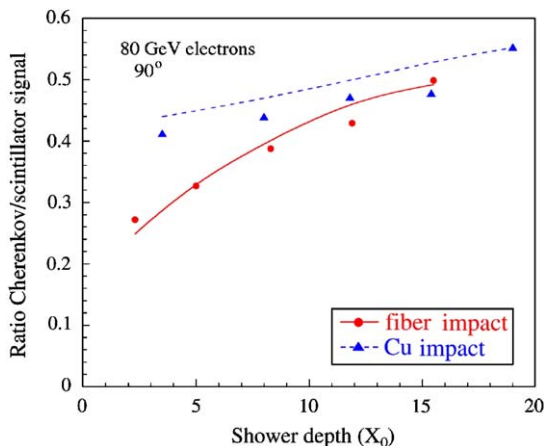


Fig. 15. Ratio between the average Cherenkov and scintillator signals from 80 GeV electron showers, as a function of shower depth. The electrons entered the detector at an angle $\phi = 90^\circ$ with the fiber direction. Results are given separately for events in which the electrons entered the detector in a plane containing only copper, or in a plane containing the active material. The curves represent the results of Monte Carlo simulations.

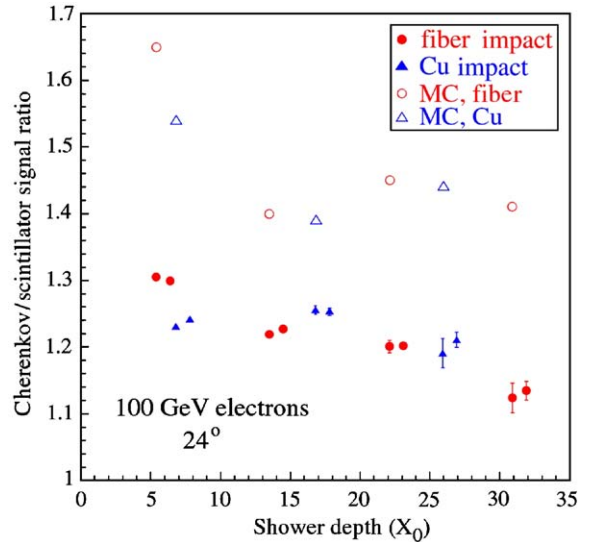


Fig. 16. Ratio between the average Cherenkov and scintillator signals from 100 GeV electron showers, as a function of shower depth. The electrons entered the detector at an angle $\phi = 24^\circ$ with the fiber direction. Results are given separately for events in which the electrons entered the detector in a plane containing only copper, or in a plane containing the active material. Results of Monte Carlo simulations are given as well.

traversed by the shower axis, for event samples in which the electrons entered the detector in the fiber and copper planes, respectively. The data show that this ratio gradually increases as the shower develops. This reflects the gradually diminishing role of the collimated shower component, to which the Cherenkov fibers are insensitive and the scintillating fibers are sensitive. The differences between the ratios for the two different event samples are commensurate with the differences between the total signals (Figs. 11c and d). They only play a role in the early part of the showers, beyond the shower maximum differences resulting from the impact point of the beam particles vanish. The described characteristics are well described by our Monte Carlo simulations (see Section 5.4).

Fig. 16 shows results for electrons entering the detector at $\phi = 24^\circ$. These measurements also probe the late stages of the em shower development. In this case, differences resulting from the impact point of the beam particles are much less

pronounced than at $\phi = 90^\circ$. This is because at this angle, some fraction of the collimated shower component falls within the numerical aperture of the Cherenkov fibers, and thus contributes to the Cherenkov signals (see also Figs. 11a and b). The ratio of the average Cherenkov and scintillator signals tends to decrease as the shower develops, by about 10% over the depth range covered by these measurements. Similar results were obtained for electron showers at other energies.

These results imply that in the late stages of the shower development, the Cherenkov signals are smaller than expected on the basis of the energy deposit profile. This is no surprise, because as the shower develops, the average energy of the shower particles decreases. Therefore, an increasing fraction of these particles fall below the Cherenkov threshold. Particles with energies below this threshold do produce scintillation light, but no Cherenkov light.

As illustrated in Fig. 16, the Monte Carlo simulations do not describe these experimental results as well as those obtained for perpendicular (90°) showers. The overall tendency that the \check{C}/S signal ratio decreases as the shower develops is reproduced by these simulations, but the simulated values of this ratio are significantly larger than those observed experimentally. The main difference between the 24° data and those obtained at 0° and 90° is that, at 24° , the early, collimated shower component does contribute to the Cherenkov signals. However, this contribution depends sensitively on details such as the angle of incidence of the beam particles and the numerical aperture of the fibers. We found that small changes in the values of these parameters led to substantial changes in the simulated \check{C}/S signal ratio. In the Monte Carlo studies, $O(10\%)$ effects were observed when the angle in the horizontal plane was changed from 24° to 22° or when the angle in the vertical plane was changed from 0.3° to 0.7° . The results were even more sensitive to the numerical aperture of the Cherenkov fibers. A decrease of 10% in the aperture values reduced the \check{C}/S signal ratios by 20–25%, bringing them in good agreement with the experimental data.

It may well be that the observed discrepancy with the experimental data is indeed the result of

such experimental factors, i.e. errors in the assessed values of these parameters. We are planning further measurements at other angles, and in particular at the Cherenkov angle of 46° , to investigate this issue.

5.4. Monte Carlo simulations

Stand-alone EGS4 Monte Carlo simulations of em showers developing in copper showed that for 80 GeV electron showers, $\sim 15\%$ of the total energy is deposited within a distance of 1 mm from the shower axis. This singularity in the energy deposit profile, which confirms our observations (see Fig. 9) has a variety of important practical consequences, several of which are discussed in another paper [2]. Among these, we mention:

- The sampling fraction, and thus the calorimeter response, depends on the impact point of the particles. It is larger for particles entering the detector in a fiber plane than for particles entering in the copper in between such planes. This phenomenon is clearly observed in Fig. 12.
- The em energy resolution exhibits deviations from $E^{-1/2}$ scaling, since these response variations are, in first approximation, independent of the electron energy.

Experimentally, we observed that both effects are strongly dependent on the angle between the direction of the incoming particles and the fibers. At small angles, both effects are much more dominant for the scintillation signals than for the Cherenkov ones [2]. The latter observation corroborates the explanation of the shower profile differences given in Section 5.1.

GEANT3 simulations of em shower development in the DREAM calorimeter (see Section 4.2) were used to calculate details of the radial and depth distributions of both Cherenkov light and scintillation light, for 40 and 80 GeV electrons. The radial distribution of Cherenkov and scintillation light at three different electron incident angles (ϕ, θ) are shown out to a radius of 30 mm in Figs. 17a and b, respectively. Experimental data were taken for two of these detector orientations,

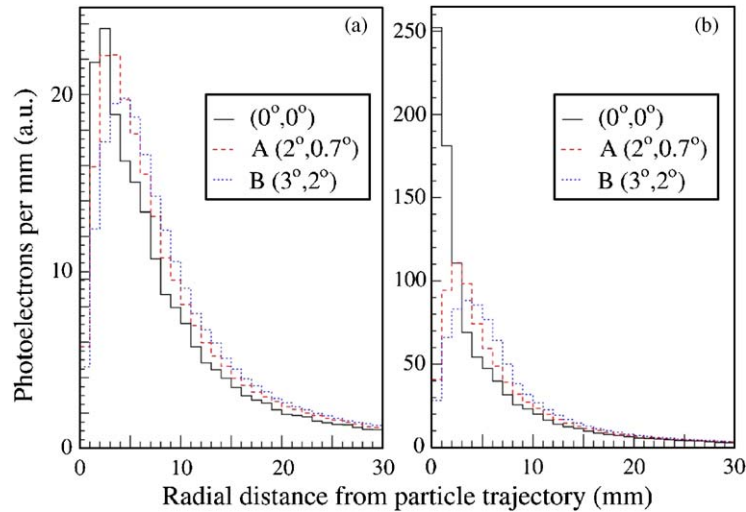


Fig. 17. Radial density of Cherenkov (a) and scintillation (b) light at three angles of incidence (ϕ, θ). Results of GEANT3 simulations for 80 GeV electrons incident on the DREAM calorimeter.

and we have simulated the $\phi = \theta = 0$ orientation for completeness.

It is clear (in this idealized simulation) that at a beam angle of $\phi = \theta = 0$, electrons channel geometrically down both types of fibers. In the case of the scintillating fibers, this leads to an enhanced signal at small radii (inside 4 mm) as the electrons travel large path lengths inside the fiber. In the case of the Cherenkov fibers, however, an electron channeling down a fiber emits Cherenkov light at an angle of about 46° with respect to the particle direction. Since the numerical aperture of these fibers is 0.33 (quartz) or 0.50 (plastic), only photons traveling at angles smaller than 20° (quartz) or 30° (plastic) with the fiber axis can be trapped. Thus, no Cherenkov photons are captured in the fiber for a channeling electron.

The differences between the radial profiles measured with the two types of fibers are of course most spectacular when the incoming particles travel exactly in the fiber direction, i.e. for the $(0^\circ, 0^\circ)$ orientation. As the angle between the incoming particles and the fibers increases, the smearing effects we observed experimentally (Fig. 9) immediately start to play a role, as illustrated by the difference between the radial scintillator profiles in the orientations $(0^\circ, 0^\circ)$ and A $(2^\circ, 0.7^\circ)$. Yet, also at angles of a few degrees,

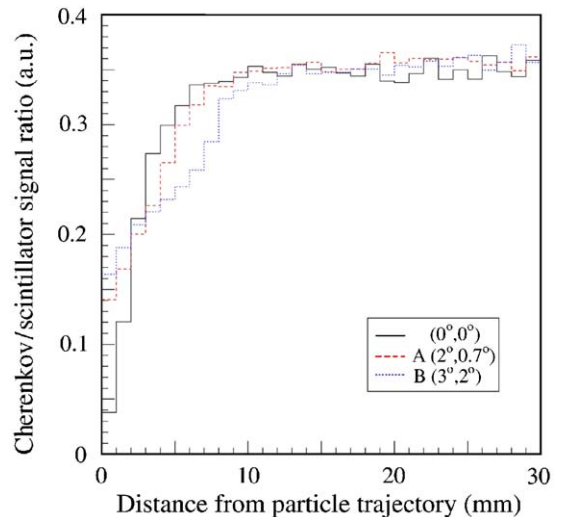


Fig. 18. The ratio of the Cherenkov signal to the scintillator signal as a function of the radial distance from the particle's trajectory, for 80 GeV electrons entering the DREAM calorimeter at three different angles (ϕ, θ). Results of GEANT3 simulations.

the differences between the radial profiles measured with the two types of fibers remains substantial, as illustrated in Fig. 18.

This figure shows the ratio of the signals from the Cherenkov and the scintillating fibers, as a

function of the radial distance (r) from the particle’s trajectory. For the orientation in which we measured the profiles, A ($2^\circ, 0.7^\circ$), the Cherenkov signal from the region $r < 2$ mm is reduced to $\sim 45\%$ of its value in the region $10 < r < 15$ mm, when we use the scintillator signals for normalization. Experimentally, we measured this depletion to be smaller: The ratio of the Cherenkov and scintillator signals for $x < 2$ mm is $\sim 70\%$ of the value in the region $10 < x < 15$ mm. Most likely, this difference stems from the fact that the experimental results concern $\Delta E/\Delta x$ profiles, instead of the simulated dE/dr ones. As discussed in Section 5.1, contributions from regions with $r > x$ (the shower *periphery*) increasingly “pollute” the results as x decreases (see also Fig. 4). As a result, differences between the shower profiles measured with Cherenkov light and scintillation light, which originate from processes close to the shower axis, tend to be underestimated on the basis of our experimental data.

The absence of a Cherenkov signal from the early, highly collimated shower component is also reflected in the longitudinal shower profiles. Fig. 19 shows the results of simulations for 80 GeV electrons entering the DREAM calorimeter, averaged over the three angles of incidence mentioned above. The ratio of the two signals shows a very

significant depletion of Cherenkov photons from the early part of the shower (Fig. 19b). This depletion is believed to be one of the factors responsible for the fact that a non-linearity observed for the scintillator signals from electromagnetic showers in DREAM was absent for the Cherenkov channel [2].

The longitudinal profiles measured in the present study are also affected by the mentioned depletion. When the beam particles enter the DREAM calorimeter at 90° , the Cherenkov fibers are as “blind” to the early, collimated shower component as at 0° . The observed gradual increase of the \check{C}/S signal ratio with the shower depth (Fig. 15) is a consequence of this.

A second effect apparent from the 0° simulations of longitudinal shower development (Fig. 19b) takes place in the shower tails. Beyond the shower maximum, the ratio of the Cherenkov and scintillator signals gradually decreases. This phenomenon is also experimentally observed in the 24° data (Fig. 16), which probe the tails of the longitudinal shower development. It underscores the importance of low-energy shower particles in the energy deposit process. Since the Cherenkov light yield is proportional to $\sin^2 \theta_C = 1 - (n\beta)^{-2}$, the 10% reduction experimentally observed means that the average velocity of the electrons

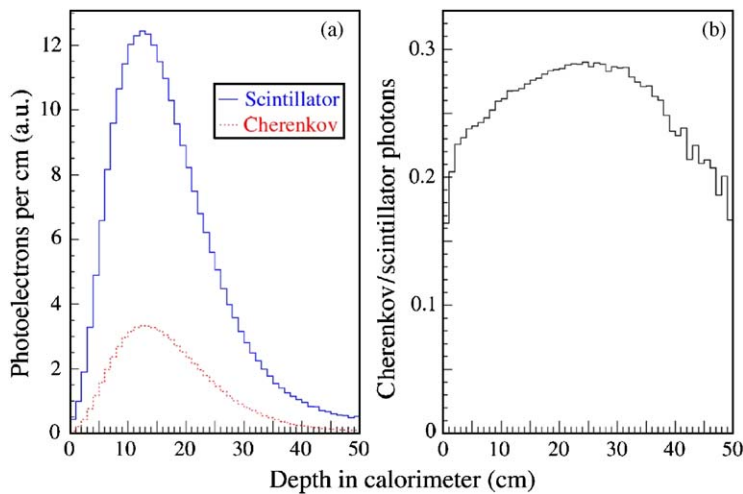


Fig. 19. The longitudinal development of the Cherenkov and scintillation signals (a) and the ratio of both signals as a function of depth (z). Results of GEANT3 simulations for 80 GeV electrons entering the DREAM calorimeter at a small angle with the fibers.

contributing to the calorimeter signals is $\beta \approx 0.95$, which corresponds to a kinetic energy of ~ 1 MeV.

6. Conclusions

We have measured lateral and longitudinal electromagnetic shower profiles in a copper-based calorimeter equipped with two active media. Scintillating fibers measured the energy deposit profile, while clear fibers measured the profile of the shower particles capable of generating Cherenkov light. We observed two types of differences between these profiles:

- (1) The early, strongly collimated shower component, dominated by e^+e^- pairs produced by photons radiated by the incoming particle is not contributing at all to the Cherenkov signals, when the beam particles enter either along or perpendicular to the fiber direction. This is because the Cherenkov light generated by this shower component falls in these cases outside the numerical aperture of the fibers. This effect is clearly visible, both in the measured lateral and longitudinal shower profiles.
- (2) In the late stages of the shower development, the Cherenkov signal is gradually depleted compared to the scintillator signal. This effect, which is also observed both radially and longitudinally, is a result of the fact that the average energy of the shower particles drops to the point where non-relativistic effects start to become significant.

Both effects are in general agreement with the results of Monte Carlo simulations, even though some details of the Cherenkov response are not perfectly reproduced by the available code when the calorimeter is oriented such that the collimated shower component does contribute significantly to the signals.

Experimental consequences for the operation of the DREAM calorimeter derive especially from the first effect. Because of the absence of contribu-

tions from the early bremsstrahlung to the Cherenkov signals, em shower detection with the Cherenkov channels of the calorimeter is more linear and the response is less sensitive to the impact point of the particles than for the scintillator channels. Also these effects are in agreement with experimental observations [2].

Acknowledgements

We gratefully acknowledge the contributions of Tracy McAskill, Vladimir Nagaslaev, Alan Sill, Veronica Stelmakh, Yunyong Wang, Erika Washington and Kim Zinsmeyer to the construction of the DREAM detector. We thank CERN for making particle beams of excellent quality available. Our beam tests would not have been possible without the help we received from Claude Ferrari and Maurice Haguenaer. We thank K. Kuroda for loaning us the fiber hodoscopes, and A. Gorin and I. Manouilov for their assistance with the data acquisition system. This study was carried out with financial support of the United States Department of Energy, under contract DE-FG02-95ER40938, and the Advanced Research Program of the State of Texas.

References

- [1] R. Wigmans, *Calorimetry—Energy Measurement in Particle Physics International Series of Monographs on Physics*, vol. 107, Oxford University Press, Oxford, 2000.
- [2] N. Akchurin, et al., *Nucl. Instr. and Meth. A* 536 (2005) 29.
- [3] N. Akchurin, et al., *Nucl. Instr. and Meth. A* 537 (2005) 537.
- [4] N. Akchurin, et al., *Nucl. Instr. and Meth. A* 533 (2004) 305.
- [5] G. Bathow, et al., *Nucl. Phys. B* 20 (1970) 520.
- [6] D. Acosta, et al., *Nucl. Instr. and Meth. A* 316 (1992) 184.
- [7] N. Akchurin, et al., *Nucl. Instr. and Meth. A* 471 (2001) 303.
- [8] W.R. Nelson, H. Hirayama, D.W.O. Rogers, EGS 4, SLAC Report 165, Stanford (1978).
GEANT—Detector Description and Simulation Tool, CERN, 1993.
- [9] N. Akchurin, R. Wigmans, *Rev. Sci. Instr.* 74 (2003) 2955.